Smart control of electromagnetically driven dosing pumps

Dipl.-Ing. Thomas Kramer, Dipl.-Ing. Martin Petzold, Prof. Dr.-Ing. Jürgen Weber

Institut für Fluidtechnik (IFD), Technische Universität Dresden, Helmholtzstrasse 7a, 01069 Dresden, Germany, E-mail: mailbox@ifd.mw.tu-dresden.de

Dr.-Ing. Olaf Ohligschläger, Dr.-Ing. Axel Müller

Thomas Magnete GmbH, San Fernando 35, 57562 Herdorf, Germany, E-Mail: info@thomas-magnete.com

Abstract

Electromagnetically driven dosing pumps are suitable for metering any kind of liquid in motor vehicles in a precise manner. Due to the working principle and the pump design, an undesired noise occurs when the armature reaches the mechanical end stops. The noise can be reduced by an adequate self-learning control of the supply energy using a position estimation and velocity control. Based on preliminary investigations /1/, a method for noise reduction is realised by using a user-friendly, tiny and cost-efficient hardware, which enables a use in series manufacturing. The method requires only a voltage and current measurement as input signals. The core of the hardware is an 8-bit microcontroller with 8 kilobytes flash memory including necessary peripherals. A smart software development enables an implementation of the entire noise reduction method onto the tiny flash memory.

KEYWORDS: dosing pump, noise reduction, velocity control, position estimation

1. Introduction

Electromagnetically driven single piston pumps are well suited for metering of different liquids in vehicles. The movement of the piston is realised by using the reluctance principle in combination with a return spring (**Figure 1**).

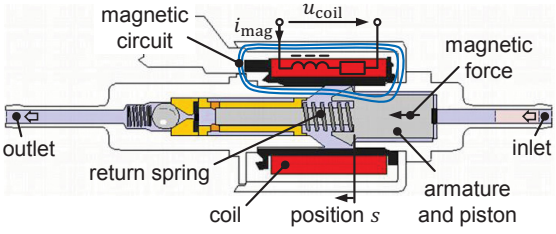

Figure 1: Design of a single piston pump

As described in /1/, an undesired noise occurs due to the working principle and the pump design. The noise level depends on the armature velocity at the end stops. A reduction of the end stop velocity independently from the inputs such as supply voltage, outlet pressure and liquid properties can be achieved by using an end stop velocity control. A sensorless position estimation based on the evaluation of the position-dependent magnetic behaviour delivers the controller input. This method relies on voltage and current measurements. A modification of the pump design is not necessarily required. The described approach can be realised using simple and cost efficient electronics. The electronic circuit can be directly integrated into the pump connector or in the pump itself so that smart dosing pumps can be manufactured in series.

The focus of this paper is the implementation of the algorithm onto an 8-bit microcontroller. At first, a short introduction to the used position estimation and velocity control is given. Then, the realisation of the algorithm in hardware and software is presented. Finally, important results such as validation of estimated position, controller function, energy consumption, noise reduction and dosing accuracy are discussed.

2. Basics

2.1. Position estimation

There are several methods for sensorless determination of the armature position described in literature. Richter gives an overview of promising methods /2/. All methods take advantage of the position-dependent inductive behaviour of a magnetic coil. In dosing pumps, the analysis of the magnetic flux linkage Ψ /3/ provides the best potential for a position estimation /1/. This method uses the intrinsic correlation between magnetic flux linkage Ψ, coil current i_{mag} and position s (**Figure 7**). The magnetic flux linkage is calculated sensorless by the integration of the induced voltage as

$$\Psi = \int u_{\mathrm{ind}}\, dt + \Psi_0 = \int \left(u_{\mathrm{coil}} - R_{\mathrm{coil}} i_{\mathrm{mag}}\right) dt + \Psi_0. \tag{1}$$

2.2. Velocity control

Several approaches for the control of the armature velocity at the end stops have been investigated /4/. These are mostly known as softlanding strategies. Due to the influence of eddy currents on the position estimation /1/ and the microcontroller's limited performance, their applicability to dosing pumps is limited. An iterative learning control based on the pump's repetitive working principle is used. Thus, a simple method to achieve a reduced end stop velocity v_{f} of the forward stroke is the reduction of the power supply by an adjustable second voltage level u_{II} (**Figure 5**). The end stop velocity v_{r} of

the return stroke can be reduced by an additional voltage pulse u_{IV}. The magnetic force increases again and acts against the spring force that accelerates the armature.

Controlling the end stop velocities of the forward and return stroke is realised by a time-discrete I-controller, because the pump section of the control path (input: reduced voltage level, output: end stop velocity) behaves according to a proportional element with variable gain (no interaction of following strokes), as shown in **Figure 2** (nominal: supply voltage u_{in} = 12 V, $u_{\mathrm{II}} = u_{\mathrm{in}}$, u_{IV} = 0). In addition to that, a highly dynamic control is not necessary due to the slow change of operating parameters such as coil temperature, liquid properties and battery voltage. The following control law for the corresponding reduced voltage u_{red} is used for the end stop velocity control of forward and return stroke:

$$u_{\mathrm{red,k}} = u_{\mathrm{red,k-1}} + K_{\mathrm{I}}\left(\left|v_{\mathrm{endstop,des}}\right| - \left|v_{\mathrm{endstop,est,k-1}}\right|\right). \tag{2}$$

The controller gain K_{I} is different between forward and return stroke. The gain $K_{\mathrm{I,f}}$ for forward stroke is positive to reduce voltage level $u_{\mathrm{II}} = u_{\mathrm{red,f}}$ at higher estimated end stop velocity $v_{\mathrm{f,est}}$ as desired value $v_{\mathrm{f,des}}$. The gain $K_{\mathrm{I,r}}$ for return stroke is negative, because the voltage level $u_{\mathrm{IV}} = u_{\mathrm{red,r}}$ has to be increased for a lower absolute velocity $|v_{\mathrm{r}}|$.

Boundary conditions are a non-arrival at the forward end stop and an undesired forward motion during return stroke. A desired end stop velocity $v_{\mathrm{f,des}}$ > 0 ensures the arrival at the end stop s_{max}. A sliding motion in the return end stop is ensured by an observer, which checks the velocity development for a continuously increasing velocity with v < 0.

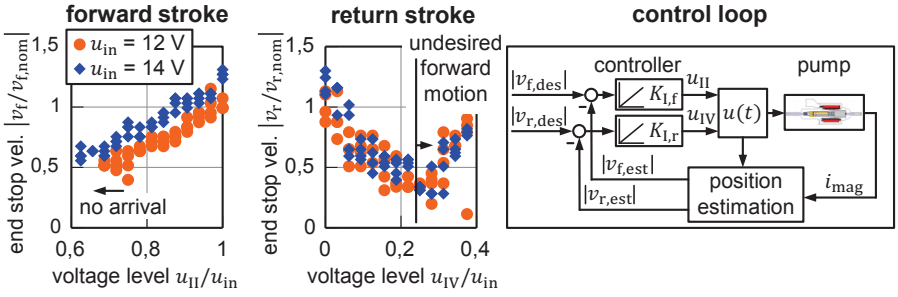

Figure 2: Transfer behaviour of end stop velocities $v_{\mathrm{f}}(u_{\mathrm{II}})$ and $v_{\mathrm{r}}(u_{\mathrm{IV}})$, simplified control loop with end stop velocity controller

3. Electronic circuit (hardware)

The realisation of the noise reduction method on small and cost efficient hardware enables a direct integration of the control principle into the pump or connector. There are three important parts required: the microcontroller (µC), the output stage and the

measurement circuit. An electronic test board containing these components in combination with an additional debugging interface was built up. The electronic test circuit and board are shown in **Figure 3**. The single components are described below.

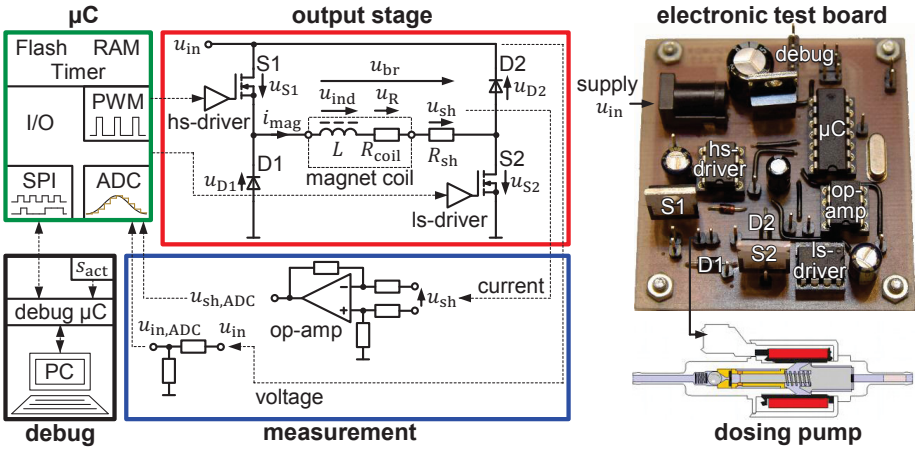

Figure 3: Electronic test circuit and build up of the test board

3.1. Microcontroller

The core of the electronic circuit is a cost-efficient 8-bit microcontroller /5/. The microcontroller is used for the execution of the algorithm and has necessary peripherals integrated. The relevant components for driving the dosing pump are

- flash memory consisting of software and maps,
- RAM for buffering values,
- 10-bit analog-digital-converter (ADC) for measuring current and voltage,
- input and output ports for debugging and electronic switch control (including a PWM output channel),
- 8-bit and 16-bit timer for timed workflow.

3.2. Output stage

The output stage of the electronic test circuit is a diagonally controlled H-bridge consisting of two fast switching MOSFETs (S1 and S2) and two Schottky diodes (D1 and D2). Three modes of current feed to the coil can be realised (**Figure 4**). Switching S1 and S2 on, the coil is excited approximately by the supply voltage u_{in} (feed mode). If only one switch is in conduction mode, the coil freewheels over the corresponding diode (freewheel mode, Figure 4 shows switch S2 in conduction mode). A fast de-energisation of the coil to achieve higher stroke frequencies can be realised by switching both switches off (fast freewheel mode). The coil freewheels driven by the supply voltage.

However, this mode is not used in the following (additional maps required). The MOSFET S2 is switched on permanently. The reduced voltage for the velocity manipulation is achieved by PWM-switching of MOSFET S1. The result is a reduced voltage in average.

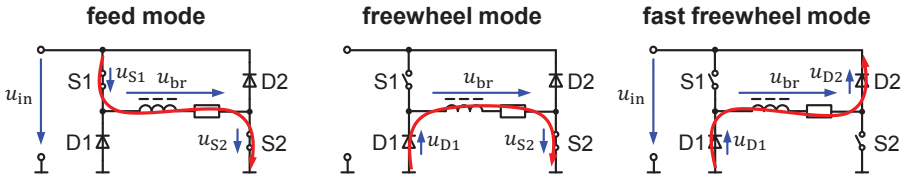

Figure 4: Modes for current feeding of the coil

The microcontroller generates the control signals for the MOSFETs. A high side driver (hs-driver, with bootstrap circuit) for S1 and a low side driver (ls-driver) for S2 gain these signals and ensure short switching times.

In addition to the normal pump driving mode, the electronic test circuit also enables the generation of maps $\Psi(i_{\mathrm{mag}}, s, u)$. The remanence flux linkage Ψ_0 cannot be determined with this test circuit, but with a modified circuit or using a FEM simulation. ANSYS Maxwell 2015.1 considers the hysteresis in major and minor loops.

3.3. Measurement circuit

The estimation algorithm needs the actual voltage and current values for flux linkage calculation according to equation (1). Therefore, the microcontroller's internal ADC is sufficient. Voltage measurement is done by a voltage divider for adapting to the ADC input range. A shunt resistor R_{sh} serves for current measurement. An operational amplifier (op-amp) interconnected as differential amplifier adapts the current proportional low voltage across the shunt resistor to the ADC input range.

3.4. Debug interface

In addition to the algorithm execution, the test circuit offers the output of selected loop and stroke data by using the SPI (serial peripheral interface) of the microcontroller. This option is provided especially for testing the functionality and output of selected results. During a loop (see 4.2), the microcontroller sends the data to a debug microcontroller (on additional board), which redirects data via RS232 to a PC (data rate: 250 kBaud). The additional debug microcontroller is also used for measuring the position signal of a sensor with its internal ADC. This enables the validation of the armature position estimation. The debug interface also provides a parameter setup via PC (controller de-/active, stroke frequency, duty cycle). The PC does not execute any part of the algorithm.

4. Algorithm implementation (software)

The complete noise reduction algorithm is implemented onto the microcontroller based on the described hardware. The challenge is an efficient implementation onto the only 8 kilobytes flash memory /5/. The algorithm and the maps are stored in this flash memory. The software contains a main procedure, which consists of single algorithm loops and is controlled by timer interrupts. This ensures an equidistant sampling for the algorithm execution, which is important for numeric flux linkage calculation. In the following, the main procedure will be described.

4.1. Main procedure

The main procedure controls the stroke by different current feed sections as well as the resistance determination, which is required for flux linkage calculation according to equation (1). Figure 5 gives an overview of the main program flow, especially showing the current feed sections.

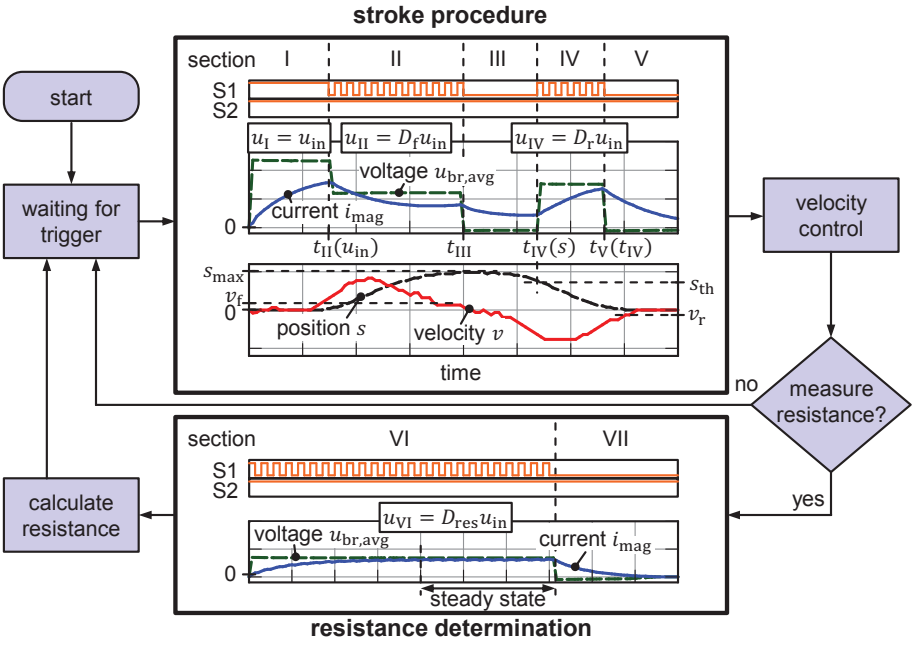

Figure 5: Main procedure with detailed stroke procedure and resistance determination

A stroke is triggered using either an external signal (additional wire required) or a short supply voltage break down (capacitors ensure continuing running of microcontroller). The test circuit is selftriggered by the software. After triggering, the stroke procedure is executed. This procedure can be devided into sections I - V for different coil excitations.

Firstly, the coil is fully supplied by the voltage u_{in} by switching S1 on (S2 is continuously on) in section I. This leads to a fast rise of magnetic force, so that the armature motion starts as fast as possible. In section II, the average coil voltage is reduced by switching S1 to PWM mode (duty cycle D_{f}) to achieve a reduced end stop velocity of the forward stroke. This section starts at time $t_{\mathrm{II}}(u_{\mathrm{in}})$, which depends on the supply voltage u_{in}. The duty cycle D_{f} is set by the forward stroke controller. The switch S1 is switched off at a constant time t_{III} in order to freewheel the coil current i_{mag} to de-energise the magnetic circuit. In this section III, the return stroke begins. When the armature position s falls below a constant threshold s_{th}, the coil is fed again to decelerate the armature motion by switching S1 to PWM mode (section IV). The corresponding duty cycle D_{r} is set by the return stroke controller. This voltage pulse ends after a defined time at $t_{\mathrm{V}}(t_{\mathrm{IV}})$. After the deceleration pulse, S1 is switched off and the current freewheels over the diode again until the current is decayed (section V).

After the stroke procedure, the velocity control is executed and sets the duty cycles D_{f} and D_{r} for the next stroke. The velocity controller is described below in chapter 4.3. It follows either a new trigger controlled stroke or a resistance determination. The last one can be divided into sections VI and VII. At first, the coil is excited by a low average voltage using PWM (duty cycle D_{res}) to ensure no stroke occurence (section VI). With the measurement of the voltage and current in steady state (Figure 5), the bridge resistance

$$R_{\mathrm{br}} = R_{\mathrm{coil}} + R_{\mathrm{sh}} \tag{3}$$

is determined. In the following section VII, the current freewheels by switching S1 off.

4.2. Algorithm loop

The main procedure consists of periodically executed algorithm loops. The algorithms for stroke procedure and resistance determination are different. In the following, only the algorithm of the stroke procedure is described. This algorithm can be divided into measurement and calculation. **Figure 6** gives an overview of the corresponding program flow for an algorithm loop including the required time in average. The real-time position estimator needs the most of the time due to the sequentiell interpolations (described in 4.2.5). An overhead time is necessary for longer calculations (required time depends on input numbers of calculation) and for the management of the current feed sections.

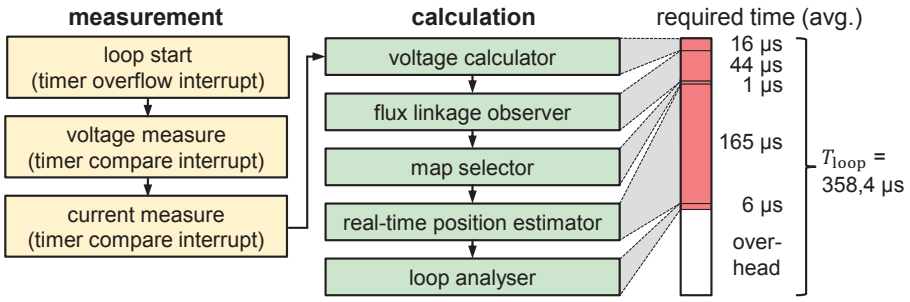

Figure 6: Program flow chart of algorithm for stroke procedure

The microcontroller works with an external 20 MHz crystal. It enables a loop time T_{loop} = 358,4 µs (sample rate: approx. 2,8 kSps), which is constant and realised by a timer overflow interrupt. The short loop time is achieved by a smart implementation of the algorithm, for example substituting clock-saving bit shifting (means division by 2^n) for division calculations as far as possible.

4.2.1. Voltage and current measurement

The aim of the algorithm is the estimation of the armature position for every loop. To achieve this, the flux linkage Ψ has to be calculated. Therefor, the induced voltage u_{ind} is required, which can be calculated by using the coil current i_{mag} and the entire bridge voltage $u_{\mathrm{br,avg}}$ (including shunt voltage u_{sh}). The current i_{mag} is measured and the brigde voltage is calculated from measured supply voltage u_{in}. The bridge voltage cannot be measured directly in a suitable manner. There could be an error by measuring a PWM signal due to the discrete sample and hold time. So the first step in every loop is the measurement of the supply voltage u_{in} and the current i_{mag}. The microcontroller's ADC cannot measure two channels ($u_{\mathrm{in,ADC}}$ and $u_{\mathrm{sh,ADC}}$) at the same time. Hence, a smart definition for the measuring points is required to ensure a suitable flux linkage calculation. Therefore, the measurements are triggered by timer compare interrupts for defined measuring points. With both measurements finished, the calculation part starts.

4.2.2. Voltage calculator

After the measurement, the effective voltage $u_{\mathrm{br,avg}}$ across the bridge is calculated from the measured supply voltage u_{in}. In the case of PWM switching of S1 (duty cycle D), both feed and freewheel mode (Figure 4) are used /6/. The effective bridge voltage is determined using average voltage of both modes according to the Kirchhoff law with

$$u_{\mathrm{br,avg}} = D(u_{\mathrm{in}} - u_{\mathrm{S1}} - u_{\mathrm{S2}}) + (1 - D)(-u_{\mathrm{D1}} - u_{\mathrm{S2}}). \quad (4)$$

The voltages u_{S1} and u_{S2} are the voltage drops over the switches S1 and S2 (Figure 4). By using MOSFETs with a low forward resistance, these voltage drops are negligible. The diode voltage drop u_{D1} is not negligible, although Schottky diodes for low power losses are used. Rather, there is a non-linear correlation between voltage u_{D1} and current i_{mag}. To consider this, an additional map $u_{D1}(i_{mag})$ is stored inside the flash memory. Corresponding to the actual current, the diode voltage drop can be determined.

The PWM frequency has to be a compromise between current ripple (low frequencies, influences position estimation) and influence of the switching behaviour of the MOSFETs (high frequencies, deviations in the pump's applied duty cycle). A PWM frequency of approx. 10 kHz with a resolution of 128 steps (using 8-bit timer) is suitable and is used.

4.2.3. Flux linkage observer

For the position estimation, the flux linkage is numerically integrated using calculated brigde voltage, measured current and prior determined resistance with

$$\Psi_k = \Psi_{k-1} + \left(u_{br,avg,k} - R_{br} i_{mag,k}\right) \cdot T_{loop}. \quad (5)$$

4.2.4. Map selector

The position estimation method is generally based on a map $\Psi_{map}(i_{map}, s_{map})$, which describes the position-dependent magnetic behaviour. However, there are eddy currents in the electrically conductive magnetic material depending on the current gradient and thus on the supply voltage. Extended maps $\Psi_{map}(i_{map}, s_{map}, u_{map})$ according to the effective bridge voltage $u_{br,avg}$ can consider eddy currents /1/, /7/. Figure 7 shows a selection from the entire map.

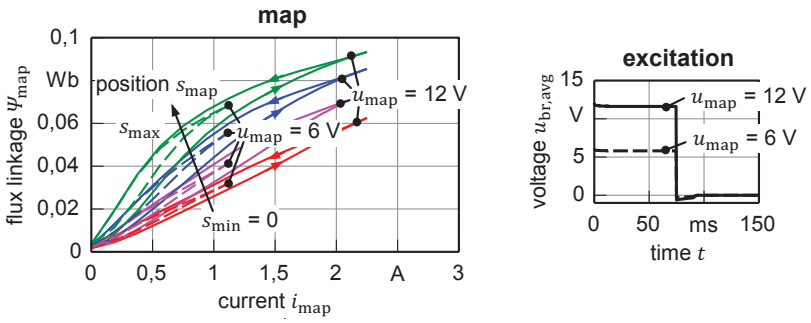

Figure 7: Selection of the stored maps $\Psi_{map}(i_{map}, s_{map}, u_{map})$ with excitation

The map as result of a measurement on the dosing pump is stored in the flash memory.

4.2.5. Real-time position estimator

With the knowledge of the actual coil current, the effective voltage and the calculated flux linkage, the position can be estimated by using linear interpolation. First, the map section $i_{\mathrm{map,i}} \leq i_{\mathrm{mag,k}} < i_{\mathrm{map,i+1}}$ is interpolated according to the effective voltage $u_{\mathrm{br,avg}}$. Second, this map section is interpolated according to $i_{\mathrm{mag,k}}$. This provides values of flux linkage $\Psi_{\mathrm{map}}\left(i_{\mathrm{mag,k}}, s_{\mathrm{map}}, u_{\mathrm{br,avg}}\right)$ corresponding to the positions s_{map} used for map generation. Finally, the position s_{est} is estimated by an interpolation using the calculated flux linkage $(\Psi_{\mathrm{k}} + \Psi_{\mathrm{k-1}})/2$ according to the current measuring point $i_{\mathrm{mag,k}}$. The armature velocity is achieved by derivation of the estimated position by

$$v_{\mathrm{est,k}} = \left(s_{\mathrm{est,k}} - s_{\mathrm{est,k-1}}\right)/T_{\mathrm{loop}}. \tag{6}$$

With the information of the position $s_{\mathrm{est,k}}$ and the velocity $v_{\mathrm{est,k}}$, the loop can be analysed.

It must be pointed out that an estimation error occurs directly after a voltage step /1/. By dropping values after the step and interpolating the missing values as soon as the position estimation works fine (determined prior by comparison of estimated and measured position), the error can be minimised. However, the debug board (used for generating results in chapter 5) outputs the estimated values without interpolation.

4.2.6. Loop analyser

The required inputs for the velocity control are determined by the loop analyser. These are especially the end stop velocities of the forward and return stroke. The end stop velocity of the forward stroke is determined shortly before the end stop ($s \approx 0{,}95\ s_{\mathrm{max}}$). This also considers a possible error of the estimation due to flux linkage calculation and map interpolation. Within a wide range of the supply voltage u_{in}, it can be assumed, that it is approx. the end stop velocity (deviations at u_{in} = 10 V, see **Figure 10**). The end stop velocity of the return stroke is determined in the same way ($s \approx 0{,}05\ s_{\mathrm{max}}$). Furthermore, the loop analyser observes the boundary conditions for the velocity control (described in 2.2) and the threshold position s_{th} for the additional pulse during return stroke.

4.3. Velocity controller

After the stroke is done, the iterative learning controller works and sets the duty cycles D_{f} and D_{r} for the next stroke according to the control law (equation (2)). In order to reduce oscillating duty cycles, a dead control range is used. If the determined end stop velocity is in this range, the duty cycle must not be changed. This is necessary due to the low resolution of the duty cycle.

5. Results

By using the above described hardware and software, the pump was actuated to analyse its behaviour. The results of different experiments are described below.

5.1. Validation of estimated position

In addition to the estimated position, a real position signal was measured on a modified dry dosing pump. This enables a validation of the estimated position to ensure correct input values for the velocity control. **Figure 8** shows the estimated and measured position for nominal and noise-reduced settings using the dry dosing pump.

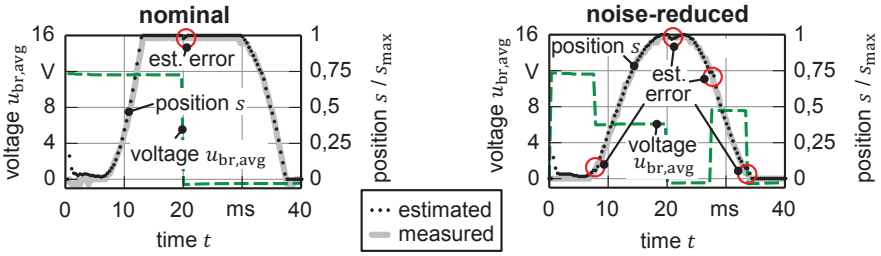

Figure 8: Validation of estimated position for nominal and noise-reduced settings

The results show a good agreement between estimated and measured position. The estimation error after switching to another voltage level can be seen (4.2.5).

5.2. Velocity control and energy consumption

The functionality of the velocity control is shown with the help of the transient behaviour. Starting with a nominal stroke (D_{f} = 1, D_{r} = 0), the controller is activated at stroke no. 20, as shown in **Figure 9**. Based on the I-controller and the pump's proportional transfer characteristic with variable gain, an approx. PT1 behaviour results for the end stop velocities of the forward and return stroke.

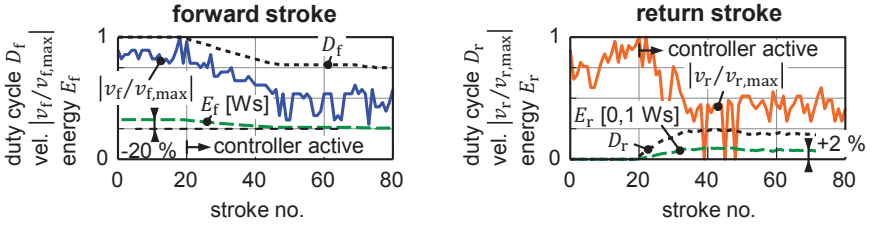

Figure 9: Transient behaviour of velocity control and energy consumption (u_{in} = 12 V)

Figure 9 shows the reduction of the end stop velocities and the energy consumption (forward stroke: energy E_{f} of section I and II, return stroke: energy E_{r} of section IV, see

Figure 5). Although the voltage pulse at return stroke needs additional energy in contrast to the nominal excitation, 18 % of energy can be saved. The energy saving increases with the supply voltage u_{in} due to more unused overhead energy in nominal excitation.

5.3. Noise reduction and dosing accuracy

Depending on the armature velocity at the end stop, the noise emission of the pump was determined. Figure 10 shows the noise characteristic of the pump for different armature velocities.

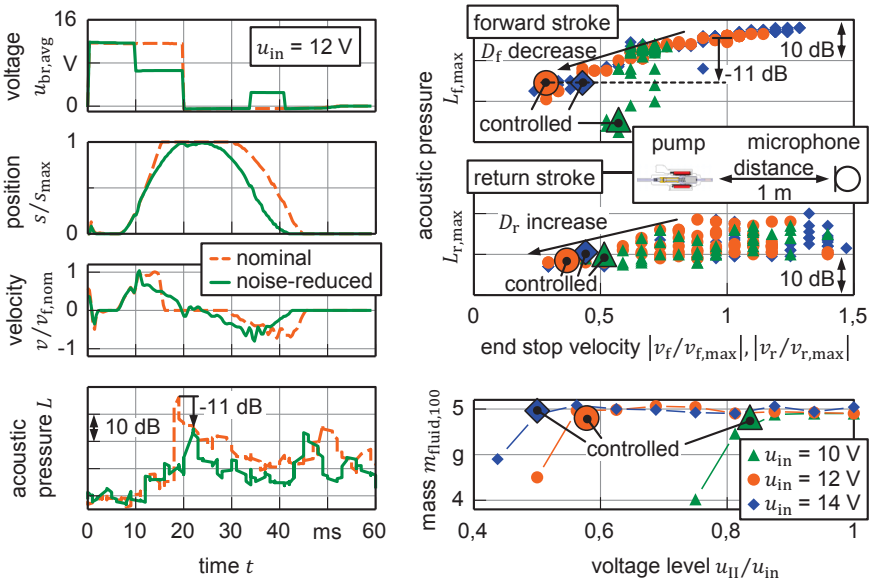

Figure 10: Noise development for a nominal and a controlled stroke (left), noise level $L_{\mathrm{f,max}}(v_{\mathrm{f}})$ and $L_{\mathrm{r,max}}(v_{\mathrm{r}})$ (right top), delivered liquid mass $m_{\mathrm{fluid,100}}(u_{\mathrm{II}})$ per 100 strokes (right bottom)

The variation of the velocity was realised by processing and controlling the estimated position signal of the armature. The end stop velocity of the forward stroke has a significant influence on the noise emission of the pump. The halving of the armature velocity on the forward end stop reduces the acoustic pressure by 11 dB. A reduction of the acoustic pressure can also be seen for the reduction of the end stop velocity of the return stroke. However, the noise emission of the return stroke appears to be superimposed by other effects. All measurements show an identical delivery mass per 100 strokes. For this reason, it is assumed that the armature always reaches the end stops. Applicating the presented smart control strategy, the high dosing accuracy of the pump can be remained.

6. Conclusion and outlook

In order to reduce the noise of magnetically driven dosing pumps, a small and cost-efficient electronic test circuit has been developed and build up. It includes a microcontroller with only 8 kilobytes flash memory. The noise reduction method is based on a position estimation and velocity control, which is implemented in the microcontroller. The investigations show anticipated results, especially a noise reduction up to 11 dB at the forward end stop and a reduction of the energy consumption up to 18 % (for nominal supply voltage u_{in} = 12 V).

The cost-efficient hardware can be minimised to a few square centimetres by using SMD components and can be easily integrated into the pump or pump connector, which offers a manufacturing in series. The investigated noise reduction method can be used for further similar working solenoids.

7. Acknowledgements

The presented research is mainly part of the project KF2452603RU3/KF3167601RU3 – “Entwicklung einer neuartigen Apparatur zur Dosierung von Biokraftstoffen”, which is funded by the Federal Ministry for Economic Affairs and Energy, Germany within the ZIM programme.

Supported by:
Federal Ministry for Economic Affairs and Energy
on the basis of a decision by the German Bundestag

8. References

/1/ Kramer, T.; Petzold, M.; Richter, S.; Weber, J.; Ohligschläger, O. and Müller, A.: Investigations on position estimation and motion manipulation of electromagnetic driven dosing pumps using co-simulation. ASME/Bath Symposium on Fluid Power & Motion Control, Bath, England, UK, September 10-12, 2014

/2/ Richter, S. and Weber, J.: Sicherheitsorientierte Zustandsüberwachung an elektromagnetisch betätigten Ventilen. Informationsveranstaltung des Forschungsfonds des Fachverbandes Fluidtechnik im VDMA, Frankfurt/Main, Germany, June 26, 2013

/3/ Kallenbach, M.: Entwurf von magnetischen Mini- und Mikroaktoren mit stark nichtlinearem Magnetkreis. Dissertation, Technische Universität Ilmenau, Ilmenau, Germany, 2005

/4/ Glück, T.: Soft Landing and Self-Sensing Strategies for Electromagnetic Actuators. Dissertation, Technische Universität Wien, Wien, Austria, 2013

/5/ Atmel Corporation: 8-bit Microcontroller with 2K/4K/8K Bytes In-System Programmable Flash, ATtiny84A. Datasheet, June, 2012

/6/ Leiber, T.; Kallenbach, M.: Verfahren zur Bestimmung der Position eines Ankers/eines Ventils. Patent, DE10020896A1, Germany, Filling Date: April 29, 2000

/7/ Müller, A.; Kramer, T.; Petzold, M.; Weber, J.; Ohligschläger, O.: Verfahren zur Steuerung einer elektromagnetisch angetriebenen Hubkolbenpumpe und Vorrichtung zur Ausführung des Verfahrens. Patent, DE102014012307B3, Germany, Filling Date: August 19, 2014

9. Nomenclature

D	duty cycle	-
E	energy	Ws
i	current	A
K	controller gain	-
L	acoustic pressure	dB
L	inductance	H
m	mass	g
R	resistance	Ω
s	position	m
t	time	s
T	time period	s
u	voltage	V
v	velocity	m/s
Ψ	magnetic flux linkage	Wb